Journal of
Materials Chemistry A

Materials for energy and sustainability

rsc.li/materials-a
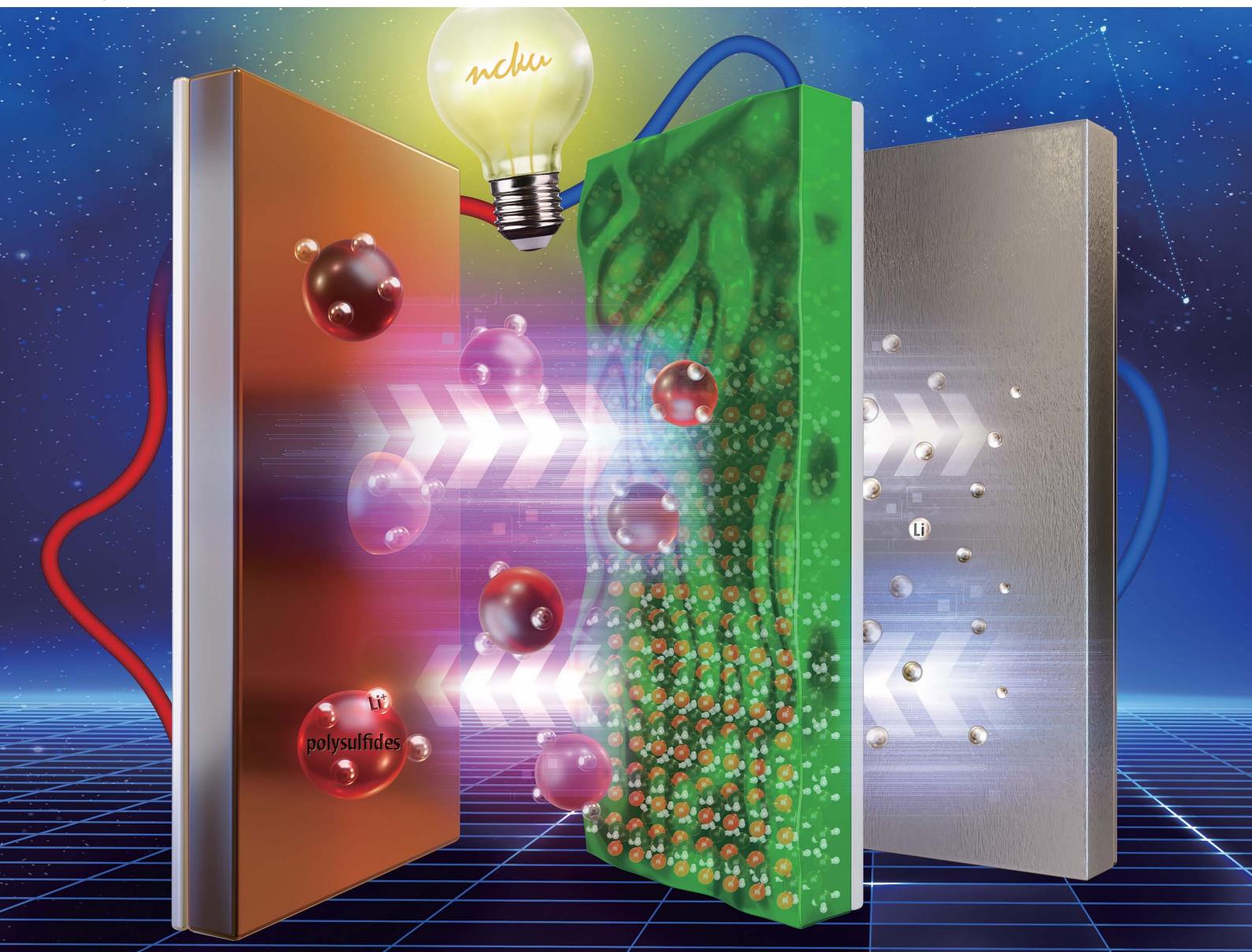
ROYAL SOCIETY
OF **CHEMISTRY**

PAPER
Li-Ling Chiu and Sheng-Heng Chung
Composite gel-polymer electrolyte for high-loading
polysulfide cathodes

Check for updates

Composite gel-polymer electrolyte for high-loading polysulfide cathodes†

Li-Ling Chiu[a] and Sheng-Heng Chung [ID] *[ab]

Lithium–sulfur batteries with a high-capacity cathode and high cell energy density have been regarded as next-generation energy-storage systems because of their suitability for high-energy-density devices with a low cost. However, the intermediate lithium polysulfides easily dissolve in liquid electrolytes and irreversibly diffuse from the cathode. In this study, we develop a high-loading polysulfide cathode featuring a polymethyl methacrylate (PMMA)-based gel-polymer electrolyte (GPE). The PMMA-based GPE inhibits the diffusion of liquid polysulfides by the strong chemical bonding between the carbonyl groups of the GPE and lithium sulfides, while offering high lithium-ion transfer for the high-loading cathode to attain outstanding electrochemical performance. Moreover, to investigate and increase the lithium-ion conductivity of the GPE, lithium bis(trifluoromethanesulfonyl)imide (LiTFSI) is mixed with PMMA at five concentrations. Material and electrochemical analyses reveal that under a high sulfur loading of 4 mg cm^{-2}, the cell with the PMMA-based GPE containing 90 wt% PMMA and 10 wt% LiTFSI exhibits the lowest impedance and highest electrochemical utilization and stability. In addition, the PMMA-based GPE allows the cell to attain higher sulfur loadings (8 and 10 mg cm^{-2}), while exhibiting a high areal capacity of 7.1 mA h cm^{-2} and a high energy density of 15 mW h cm^{-2}. Therefore, the PMMA-based GPE enhances the electrochemical stability and improves the efficiency and safety of the high-loading polysulfide cathode, which are the key factors for high-energy-density lithium–sulfur cells.

Introduction

Given the limited future increase of the charge-storage capacity and the energy density of current lithium-ion batteries, rechargeable batteries with novel electrochemistry are increasingly being developed to meet the requirements of electronic devices.[1] The lithium–sulfur battery is a promising next-generation energy-storage technology because the associated electrochemical reaction can generate two electrons per sulfur (16Li + 8S → 8Li$_2$S).[2] Thus, the sulfur cathode can generate a high theoretical charge-storage capacity and battery energy density of up to 1675 mA h g^{-1} and 2500 W h kg^{-1}, respectively, which are ten times and three to five times those of commercial lithium-ion batteries.[2,3] Moreover, unlike transition metal oxide cathode materials used in lithium-ion batteries, sulfur is abundant and low cost.[3] However, the insulating properties of sulfur (10^{-30} S cm^{-1}) and the low conductivity of the lithium–

sulfur battery discharge product (*i.e.*, Li$_2$S, 10^{-14} S cm^{-1}) deteriorate the electrochemical performance of the cell.[4–6] To tackle this problem and enhance the electrochemical performance and utilization of active materials, numerous researchers have combined sulfur with additional carbon materials,[7,8] ceramics,[9] metals,[10] or conductive polymers[11–13] to improve the charge transfer and reaction kinetics of the resulting composite sulfur cathodes.

Besides the insulating nature of the solid active material, an additional problem is that lithium polysulfide as the intermediate product is a liquid active material with high solubility in liquid electrolytes, which can rapidly degrade the reversible capacity and stability of the cell. Thus, polymers have been widely used in battery research as energy materials, separators, and interlayers.[14,15] Solid-polymer electrolytes (SPEs) and gel-polymer electrolytes (GPEs) are promising solutions to inhibit the dispersal of liquid-state polysulfides and improve the stability of lithium–sulfur batteries.[16,17] Although SPEs can inhibit the diffusion of liquid polysulfides, the low conductivities and high room-temperature resistance of polymers still limit the development of SPEs.[18] Polymer matrices have high affinity toward liquid electrolytes, which can reduce interfacial resistance;[19] therefore, many researchers have reported that GPEs such as polyethylene oxide,[20] polyacrylonitrile,[21] polymethyl methacrylate (PMMA),[22] and poly(vinylidene fluoride-*co*-hexafluoropropylene)[23] can inhibit the diffusion of lithium

[a]Department of Materials Science and Engineering, National Cheng Kung University, Tainan 701, Taiwan

[b]Hierarchical Green-Energy Materials Research Center, National Cheng Kung University, Tainan 701, Taiwan. E-mail: SHChung@gs.ncku.edu.tw

† Electronic supplementary information (ESI) available: Material analyses with contact angles, FTIR, SEM, and NMR for PMMA-based GPEs; electrochemical analysis with discharge/charge curves, ionic conductivity, and CV analysis for the cells with PMMA-based GPEs; and supporting references. See https://doi.org/10.1039/d2ta01867e

This journal is © The Royal Society of Chemistry 2022

J. Mater. Chem. A, 2022, **10**, 13719–13726 | **13719**

polysulfide, while improving the electrochemical stability and maintaining high electrochemical utilization of lithium–sulfur cells.[19,24] In addition to the material design, in recent studies, GPEs have been investigated by wide fabrication techniques, including casting, electrospinning, functional group grafting, or additive introduction to inhibit lithium polysulfide diffusion and improve the battery electrochemical performance. Ester-based polymers that can strongly interact with lithium poly-sulfides and inhibit polysulfide diffusion have recently been reported.[22] Among the ester-based polymer candidates, PMMA (R–COO–R′) endows lithium-ion batteries with high ionic conductivity because of its good affinity for organic electrolytes.[25]

Moreover, to tackle the chemistry and engineering issues of batteries, lithium–sulfur battery cathodes require a high active-material loading and content attaining 4–10 mg cm^{-2} and 60–80 wt%, respectively. With such optimal cell-design parameters, the sulfur cathode would be able to achieve a desirable electrochemical performance with high areal capacity and energy density.[26–28] Thus, GPEs that have high ionic conductivity and inhibit the diffusion of liquid polysulfides would be useful for high-loading sulfur cathodes to attain high utilization of the active material and retain liquid polysulfides in the cathode region of the cell.

Herein, we addressed the above-mentioned issues in GPEs and in lithium–sulfur technology by developing a PMMA-based GPE to allow a high-loading polysulfide cathode with enhanced electrochemical utilization and reversibility. We first fabricated the PMMA-based GPE with PMMA and lithium bis(tri-fluoromethanesulfonyl)imide (LiTFSI) integrated to a polymeric separator. PMMA, which features a carbonyl group (–C=O), has high binding energies to liquid polysulfides and Li$_2$S.[29] LiTFSI can improve the ionic conductivity of GPEs.[20] The polymeric separator offers the skeleton of the GPE membrane. We investigated five different concentrations of LiTFSI (i.e., 0, 5, 10, 15, and 20 wt%) to compare the material characteristics and electrochemical performances of different PMMA-based GPEs, which further demonstrated the optimal GPE design. Our analytical results confirm that the PMMA-based GPE with 90 wt% PMMA and 10 wt% LiTFSI provided the cell with the highest initial discharge capacity (1038 mA h g^{-1}) and best electrochemical performance at a high sulfur loading of 4 mg cm^{-2} and C-rate of C/10. Subsequently, to prove that the PMMA-based GPE can inhibit liquid polysulfide diffusion, we further increased the sulfur loading to 8 and 10 mg cm^{-2}. The PMMA-based GPE demonstrated a smooth electrochemical reaction and high capacity retention. With the high electrochemical utilization and reversibility, the PMMA-based GPE allowed the high-loading polysulfide cathode to achieve a high areal capacity and a high energy density, outperforming the current standard for lithium-ion battery cathodes.

Experimental

Preparation of PMMA-based GPEs

The PMMA-based GPE was fabricated with PMMA (average M_w ~120 000 by GPC, Sigma Aldrich) and LiTFSI (99.95%, Sigma Aldrich). PMMA and LiTFSI were mixed in acetonitrile (3 mL, 99%, J. T. Baker) at five different ratios (100 : 0, 95 : 5, 90 : 10, 85 : 15, and 80 : 20 wt%) for the investigation of the GPE characteristics and their optimization. Specifically, the mixture of PMMA and LiTFSI was stirred for 24 h at room temperature to form the GPEs. Then, the homogeneous GPEs were cast on a polypropylene substrate (PP, Celgard) through a simple doctor blade casting technique and dried overnight in a vacuum oven at 80 °C, forming the PMMA-based GPE. The GPEs were subsequently cut into circular disks of a uniform diameter of 19 mm. The resulting PMMA-based GPE had a good electrolyte absorptivity and the electrolyte affinity as compared to the pristine polypropylene substrate as demonstrated by a contact angle experiment (Fig. S1†). The analytical results indicate that the PMMA-based GPE had a low electrolyte contact angle (36°) as compared to that of the polypropylene substrate (54°).

Material measurements

The functional groups and chemical bonding in the polymer and LiTFSI were determined via Fourier-transform infrared spectroscopy (Thermo, Nicloet), Raman spectroscopy (Raman, Renishaw), and solid-state nuclear magnetic resonance (NMR) spectroscopy (Avance III HD, Bruker). The microstructure and morphological inspection of the PMMA-based GPE was observed via field-emission scanning electron microscopy (FE-SEM, JSM-7001, JEOL).

Electrochemical performance characterization

For electrochemical analysis, the PMMA-based GPE was assembled into lithium–sulfur cells with the direct application of a high-sulfur-loading polysulfide cathode for exploring the polysulfide retention and lithium-ion transfer capabilities of our GPE. Specifically, the 1.5 M polysulfide catholyte was composed of sulfur (5 mmol, 99.5%, Alfa Aesar) and lithium sulfide (1 mmol, 99.9%, Alfa Aesar) mixed into the blank electrolyte, which contained 1.85 M LiTFSI and 0.5 M LiNO$_3$ (99.98%, Alfa Aesar) dissolved in 1,2-dimethoxyethane (55 vol%, 99+%, Alfa Aesar) and 1,3-dioxolane (45 vol%, 99.5%, Alfa Aesar). The catholyte was added onto the current collector to fabricate the high-sulfur-loading cathode simultaneously with a high sulfur loading of 4 mg cm^{-2} and content of 52 wt%. The electrochemical performances of PMMA-based GPE cells with high sulfur-loading cathodes were compared to those with 8 mg cm^{-2} and 68 wt% sulfur and 10 mg cm^{-2} and 72 wt% sulfur. Next, cells with the PMMA-based GPE were assembled in an argon-filled glove box, in which the O$_2$ and H$_2$O contents were less than 1 ppm.

The assembled cells were tested at room temperature. The voltage window of cycling performance, rate performance, and charge/discharge curves were collected using a programmable battery cycler (CT-4008-5 V–10 mA, Neware) at 1.8–2.8 V and a C-rate of C/10. Furthermore, cyclic voltammetry (CV) analysis was conducted using a potentiostat (VMP-300, Biologic) at the same working voltage, but different scan rates: 0.010, 0.015, 0.020, and 0.025 mV s^{-1}. Electrochemical impedance spectroscopy (EIS) data were recorded from 1 MHz to 10 mHz using an

13720 | J. Mater. Chem. A, 2022, **10**, 13719–13726

This journal is © The Royal Society of Chemistry 2022

impedance analyzer (SP150, Biologic), at an AC voltage amplitude of 5 mV and open-circuit voltage. Additionally, the room temperature ionic conductivity value was tested at a frequency of 1 MHz to 100 Hz. Through the equation ($\sigma = d/A \times R_{b}$) about ionic conductivity, d, A and R_{b} meant the thickness, area, and bulk resistance of the PMMA-based GPE, respectively.

Results and discussion

Material characterization of PMMA-based GPEs

Generally, the interaction between the carbonyl group and lithium-ion can be proved by using the Fourier-transform infrared (FTIR) spectrum shown in Fig. S2.† According to FTIR peak analysis, the vibrations of the carbonyl group (–C=O–) and O–Li emerged at 1650 and 570 cm^{-1} after mixing LiTFSI salts with PMMA-based GPEs. The FTIR analysis shows the material characteristics that agree with the previous research results,[30–32] and conformed the successful synthesis of our PMMA-based GPE with a PMMA matrix and lithium-ion pathway.

Moreover, the Raman spectroscopy data of the chemical interaction between PMMA and LiTFSI are presented in Fig. 1 and Table 1. The carbonyl group on PMMA strongly interacts with lithium ions.[22,25,29] The absence of the peaks of carbonyl and TFSI^{-} anion groups in the GPE sample with 10 wt% LiTFSI indicates that no redundant carbonyl groups or TFSI^{-} anion groups remained inside the GPE. In contrast, the spectrum of the PMMA-based GPE without LiTFSI featured a peak at 1729 cm^{-1} due to the absence of lithium salts, whereas the spectra of the GPEs with 15 and 20 wt% LiTFSI featured a peak at 741 cm^{-1}, indicating an overdosage of lithium salts.[33] Therefore, the LiTFSI concentration in PMMA-based GPEs is an important factor in forming a lithium-ion transfer network, and

Table 1 Raman spectroscopy peak analysis of the PMMA-based GPE

Raman band (cm^{-1})	Assignments
602	ν(C–COO), ν_{s} (C–C–O)
741	TFSI^{-}
853	ν(CH$_{2}$)
999	O–CH$_{3}$ rocking
1081	ν(C–C)
1264	ν(C–O), ν(C–COO)
1460	δ_{a} (C–H) of α-CH$_{3}$, δ_{a} (C–H) of O–CH$_{3}$
1729	ν(C=O) of (C–COO)
2848	Combination band involving O–CH$_{3}$
2957	ν_{s} (C–H) of O–CH$_{3}$ with ν_{s} (C–H) of α-CH$_{3}$ and ν_{a} (CH$_{2}$)
3001	ν_{a} (C–H) of O–CH$_{3}$, ν_{a} (C–H) of α-CH$_{3}$

10 wt% was the optimum concentration in this regard. The morphologies of the prepared PMMA-based GPE samples are shown in Fig. S3.† The GPE samples with the five LiTFSI concentrations had a uniform and smooth surface, consistent with the findings of a previous study.[22] This confirms the casting method as a suitable GPE fabrication method. Moreover, the contents of PMMA and LiTFSI would be the main factor for improving the electrochemical performance of the lithium–sulfur cell with a high-loading polysulfide cathode.

To elucidate the chemical bonding between PMMA and the LiTFSI salt, the ^{1}H and ^{7}Li solid-state nuclear magnetic resonance (NMR) spectra are shown in Fig. S4.† Solid-state NMR has less sensitivity than liquid-state NMR; therefore, the H atoms of PMMA overlapped. The ^{1}H solid-state NMR spectra (Fig. S4a†) featured broad peaks and inconspicuous shifts. Moreover, a comparison of the ^{7}Li solid-state NMR spectra of the LiTFSI salt and PMMA-based GPE indicated lithium ions connected with the carbonyl group of PMMA so that the peaks shifted leftward, as reported in previous research.[34] The interaction between the lithium ions and carbonyl groups can be expected to facilitate lithium-ion transmission in the PMMA-based GPE.

Electrochemical characterization of PMMA-based GPEs

Besides the material characteristics, the electrochemical cyclabilities of PMMA-based GPEs with the five different LiTFSI concentrations are illustrated in Fig. 2a to clarify the relationship between GPE material properties and the cell characteristics. The initial discharge capacities of the lithium–sulfur cells with the polysulfide cathode and with the PMMA-based GPEs containing LiTFSI of 0, 5, 10, 15, and 20 wt% were 862, 896, 1038, 821, and 842 mA h g^{-1}, respectively, at a C-rate of C/10, i.e., under a high sulfur loading of 4 mg cm^{-2}, and the cell with an LiTFSI concentration of 10 wt% exhibited the best electrochemical performance. Furthermore, the reversible discharge capacities of the lithium–sulfur cells with the PMMA-based GPEs having LiTFSI concentrations of 0, 5, 10, 15, and 20 wt% after 200 cycles were 318, 368, 471, 411, and 264 mA h g^{-1}, respectively. The discharge/charge curves (Fig. S5†) showed that the PMMA-based GPEs with 10 wt% LiTFSI provided the cells with the lowest polarization and highest electrochemical stability. The cycling performance indicates that the PMMA-
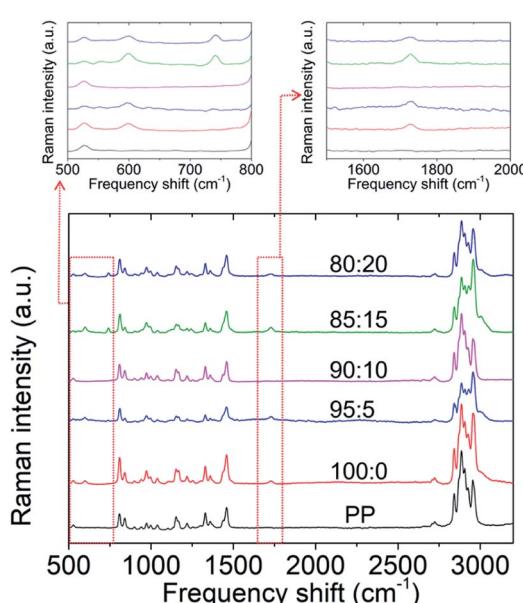
Fig. 1 Raman spectroscopy of the PMMA–based gel-polymer electrolyte (GPE).

This journal is © The Royal Society of Chemistry 2022

J. Mater. Chem. A, 2022, **10**, 13719–13726 | **13721**
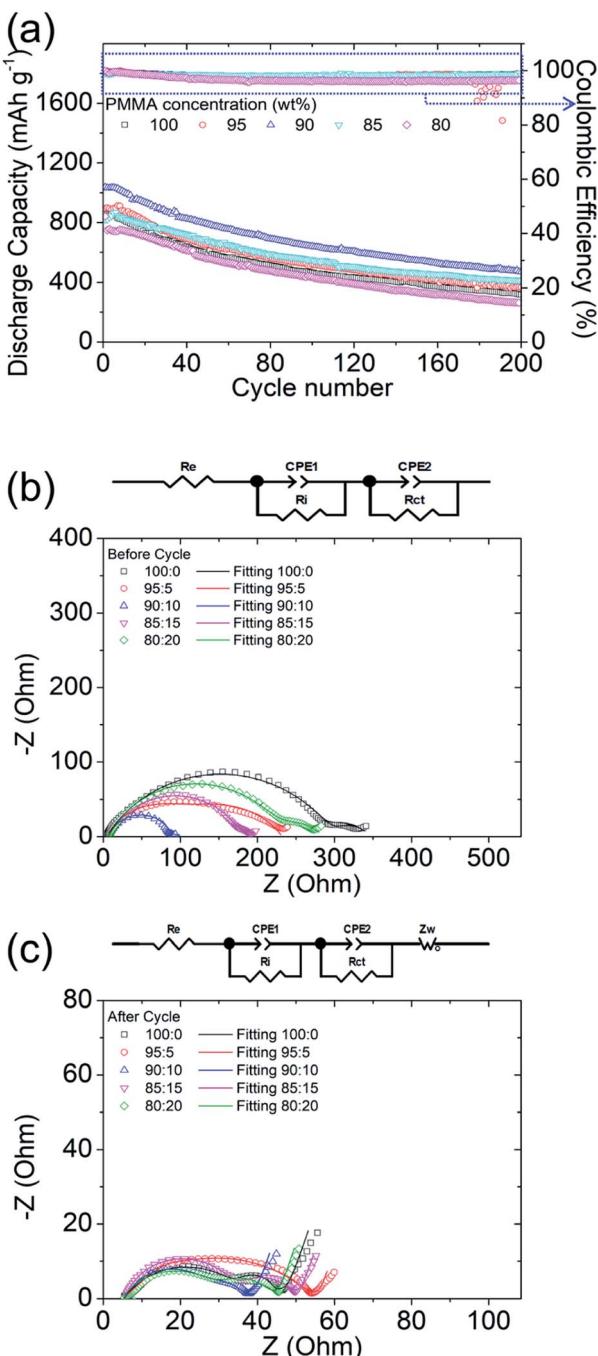
Fig. 2 Electrochemical analysis of lithium–sulfur cells with the polysulfide cathode and the PMMA-based GPEs with different PMMA : LiTFSI ratios: (a) cyclability for 200 cycles at a cycling rate of $C/10$; and electrochemical impedance spectra (EIS) (b) before and (c) after cycling.

based GPE inhibited polysulfide diffusion and optimized the stabilized polysulfides with fast lithium-ion transfer.

The experimental and analytical electrochemical impedance spectroscopy (EIS) plots of the lithium–sulfur cells with PMMA-based GPEs featuring different PMMA-to-LiTFSI ratios before and after cycling are illustrated in Fig. 2b and c. R_e, R_i, and R_{ct} represent the bulk resistance of electrodes and electrolyte,

interface resistance, and charge-transfer resistance, respectively. Warburg impedance (Z_w) is attributable to lithium-ion diffusion. Before cycling, the R_{ct} and R_i values of the lithium–sulfur cells applying the PMMA-based GPEs with PMMA : LiTFSI ratios of 100 : 0, 95 : 5, 90 : 10, 85 : 15, and 80 : 20 wt% were 294.9 and 46.9 Ω, 140.3 and 85.9 Ω, 76.8 and 14.3 Ω, 169.7 and 32.3 Ω, and 218.7 and 59.2 Ω, respectively. Therefore, the addition of the appropriate quantities of LiTFSI salt decreased the charge-transfer resistance and interface resistance, whereas the addition of excessive LiTFSI increased the charge-transfer and interface resistances and limited the electrochemical abilities of the lithium–sulfur cells. After cycling, the high frequency charge-transfer impedance of the cells was reduced, because active materials were kinetically rearranged during the electrochemical reaction. Specifically, R_{ct} at a high frequency decreased to 31.1, 46.8, 22.4, 28.7, and 25.6 Ω with PMMA : LiTFSI ratios of 100 : 0, 95 : 5, 90 : 10, 85 : 15, and 80 : 20 wt%, respectively. Moreover, the corresponding R_i at a low frequency was 6.6, 1.7, 7.7, 14.0, and 11.7 Ω, respectively.

As a result, under a high sulfur loading of 4 mg cm^{-2}, the PMMA-based GPE with an LiTFSI concentration of 10 wt% endowed lithium–sulfur cells with excellent electrochemical cyclability and stability, compared with the cells with other LiTFSI concentrations. Moreover, the PMMA-based GPE with 10 wt% LiTFSI salt exhibited the lowest electrochemical resistance in cells. All these positive features therefore affirm that the optimal LiTFSI concentration for the PMMA-based GPE in advancing lithium–sulfur cells was 10 wt%.

Lithium–sulfur electrochemistry with PMMA-based GPEs

To achieve high-electrochemical-performance energy source devices, high active-material sulfur loading of lithium–sulfur cells is essential. Moreover, to challenge the excellent material characteristics of our PMMA-based GPE, a high amount of polysulfides in the cathode is critical. Therefore, we subsequently analyzed the PMMA-based GPE with the optimized 10 wt% LiTFSI under the increasing high sulfur loadings of 8 and 10 mg cm^{-2} in the directly-used polysulfide cathode, which also evaluates the feasibility of our PMMA-based GPE.

Fig. 3a displays the electrochemical cyclabilities of high-sulfur-loading lithium–sulfur cells. The initial and reversible discharge capacities after 100 cycles of the cells with increasing high sulfur loadings of 4, 8, and 10 mg cm^{-2} were 1038 and 641 mA h g^{-1}, 797 and 502 mA h g^{-1}, and 708 and 515 mA h g^{-1}, respectively. Even the cell with an ultrahigh sulfur loading of 10 mg cm^{-2} can have a high capacity retention of 73% after 100 cycles. However, due to the electrochemical reaction of lithium–sulfur batteries, the conversion reaction of active materials between sulfur, polysulfides, and sulfides would continuously consume the electrolyte and the added LiNO$_3$ co-salt, which causes the initial decrease of the discharge/charge efficiency.[26] In our study, the cell with the PMMA-based GPE contained a high amount of sulfur and had the GPE system, which might lead to the initial decrease in the discharge/charge efficiency, while the cell then maintained a stable and high efficiency during the subsequent long cycle life. Moreover, although the

13722 | J. Mater. Chem. A, 2022, 10, 13719–13726

This journal is © The Royal Society of Chemistry 2022
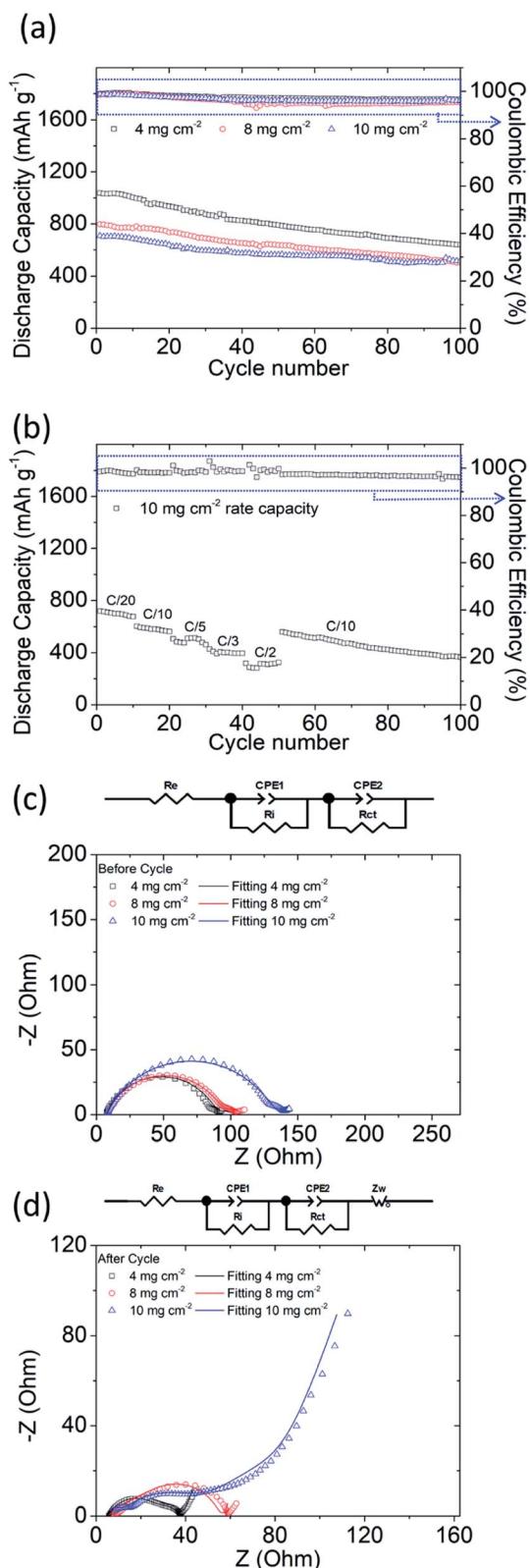
Fig. 3 Electrochemical analysis results of high-sulfur-loading cells: (a) cyclability; (b) rate performance at a sulfur loading of 10 mg cm^{-2}; and EIS images (c) before and (d) after cycling.

utilization of sulfur slightly decreased from 62%, 48%, and to 42% with the increasing high sulfur loadings from 4, 8, and to 10 mg cm^{-2} and the corresponding high sulfur contents from 52, 68, and to 72 wt%, the high-sulfur-loading polysulfide cathode eventually exhibited a high areal capacity and energy density of 7.1 mA h cm^{-2} and 15 mW h cm^{-2}, respectively. These performance values are higher than those of a commercial lithium-ion battery cathode (*e.g.*, 2–4 mA h cm^{-2} and 10–15 mW h cm^{-2}).[1–5]

Fig. 3b presents the high rate performance of the PMMA-based GPE modified lithium–sulfur cells with a high sulfur loading of 10 mg cm^{-2}. The high-loading polysulfide cathodes with the PMMA-based GPE exhibited excellent reversible discharge capacities of 717, 605, 507, 428, and 318 mA h g^{-1} at $C/20$, $C/10$, $C/5$, $C/3$, and $C/2$ ($1C = 1675$ mA g^{-1}) after 10 cycles, respectively, with high and stable discharge/charge efficiency. The cycled cell was subsequently returned to $C/10$ and subjected to 50 additional cycles. The cell still exhibited a high discharge capacity, which indicates that the PMMA-based GPE could confine liquid polysulfides in the cathode and inhibit their diffusion even if a high amount of polysulfide existed and was generated in the high-loading polysulfide cathode. In order to further support this result, we observed the cycled PMMA-based GPE composite from its anode side, which showed no trace of polysulfide diffusion and no deposition of sulfur or sulfide (Fig. S6†). Therefore, lithium–sulfur cells with a PMMA-based GPE can preserve the active material and undergo high-reversibility electrochemical reactions.

As a reference, a summary of the discharge/charge curves of the rate performance analysis is displayed in Fig. S7.† Although the cells contained a high amount of liquid polysulfide catholyte as the active material, the lithium–sulfur batteries still exhibited a smooth electrochemical reaction. To support these outstanding cell performances, we subsequently conducted electrochemical EIS and CV analysis to explore the electrochemical stability and reversibility as well as the reaction kinetics of the high-loading polysulfide cathode with the PMMA-based GPE. Moreover, we further studied the room temperature ionic conductivity values of the PMMA-based GPEs before and after soaking the electrolyte (Fig. S8†). The ionic conductivity of the PMMA-based GPE precursor was 1.66×10^{-4} S cm^{-1} before soaking the liquid electrolyte. After the GPE precursor absorbs the electrolyte, the ionic conductivity of the resulting PMMA-based GPE increases to 2.44×10^{-2} S cm^{-1}.

Fig. 3c and d present the experimental and analytical EIS data of high-loading polysulfide cathodes with the PMMA-based GPE. With increasing sulfur loadings, R_{ct} increased, attributable to the insulating properties of sulfur and the high-amount of polysulfide in the cathode. Before cycling, the cells with sulfur loadings of 4, 8, and 10 mg cm^{-2} exhibited R_{ct} values of 76.8, 85.1, and 123.7 Ω, respectively. After 100 cycles, the R_{ct} values became lower: 22.4, 26.4, and 33.5 Ω, respectively. Furthermore, the R_i values of the batteries with sulfur loadings of 4, 8, and 10 mg cm^{-2} at a low frequency changed from 14.3, 16.5, and 13.7 Ω to 7.7, 23.8, and 4.8 Ω after 100 cycles. The fresh cells shown in Fig. 3c have a high resistance because of the high amount of the insulating active material on the current

This journal is © The Royal Society of Chemistry 2022

J. Mater. Chem. A, 2022, **10**, 13719–13726 | **13723**

collector. Thus, the fresh cells showed a high impedance. After 100 cycles, as shown in Fig. 3d, the cycled active material rearranged and occupied a more electrochemically favorable position. This suggests a closer contact and better coverage between the physically stable active material on the current collector and the GPE, which results in the decrease of the impedance.[10] This further indicates that the PMMA-based GPE inhibited liquid-polysulfide diffusion and facilitated electrochemical kinetics. On the other hand, the high sulfur loading and content in the cathode also impact the resulting EIS data. The cell with the highest sulfur loading of 10 mg cm^{-2} hosted the highest amount of insulating sulfur (10 mg cm^{-2} and 72 wt%), which showed the high charge transfer resistance at high frequency. The interface resistance at low frequency would be hard to detect and covered by the high charge transfer resistance. Moreover, the high-loading sulfur cathode inevitably encountered a relatively low sulfur utilization. Thus, the resulting deposition of the converted solid active material might not be as much as that of the high-loading sulfur cathode with a sulfur loading and content of 4 mg cm^{-2} and 52 wt% and 8 mg cm^{-2} and 68 wt%. According to these two reasons, the cell with the highest sulfur loading was found with a low interface resistance and high charge transfer resistance after cell cycling.

To further clarify the enhanced electrochemical performances of the PMMA-based GPE in lithium–sulfur cells, cyclic voltammetry (CV) tests were performed at four rates (0.010, 0.015, 0.020, and 0.025 mV s^{-1}; Fig. 4a–c). The CV curves featured two cathodic peaks (i.e., $Li_2S_8/S_8 \rightarrow Li_2S_{4-8}$ and $Li_2S_{4-8} \rightarrow Li_2S_2/Li_2S$) and one broad anodic peak (i.e., $Li_2S_2/Li_2S \rightarrow Li_2S_8/S_8$). The cells were scanned two times with the increase of the scan rate, which displays each CV curve featuring two perfect reversible cycles (Fig. S9–S11†). With a high amount of sulfur of 4 to 10 mg cm^{-2} and also the increase of the corresponding sulfur content in the cathode from 52 to 72 wt%, the polarization of the cell increased as found in the CV data, which cause the differences in the oxidation peaks.[21] However, the redox reaction of our high-loading polysulfide cathodes with the PMMA-based GPE still displays high electrochemical stability and reversibility at various scan rates.

Additionally, the lithium-ion diffusion coefficient could be calculated using the Randles–Ševčík equation (Fig. S9e, S10e, and S11e†). As the high sulfur loading increased from 4 to 10 mg cm^{-2}, the lithium-ion diffusion coefficients slightly decreased from 5.27×10^{-9}–3.1×10^{-8} cm^2 s^{-1} to 2.09×10^{-9}–1.27×10^{-8} cm^2 s^{-1}, while remaining high. The retention of relatively high lithium-ion diffusion coefficients in the high-sulfur-loading cathodes indicated that the PMMA-based GPE resulted in high ionic conductivities and high lithium-ion transfer between the cathode and anode. Therefore, the PMMA-based GPE enhanced the lithium-ion transfer and inhibited polysulfide diffusion, which can limit the loss of the active material, enhance the electrochemical performance of cells, and enhance sulfur utilization.

Furthermore, we compared the studied lithium–sulfur batteries containing our PMMA-based GPE with literature-reported batteries containing other GPEs to show the development of the GPE in lithium–sulfur cells (Fig. 5). The comparison
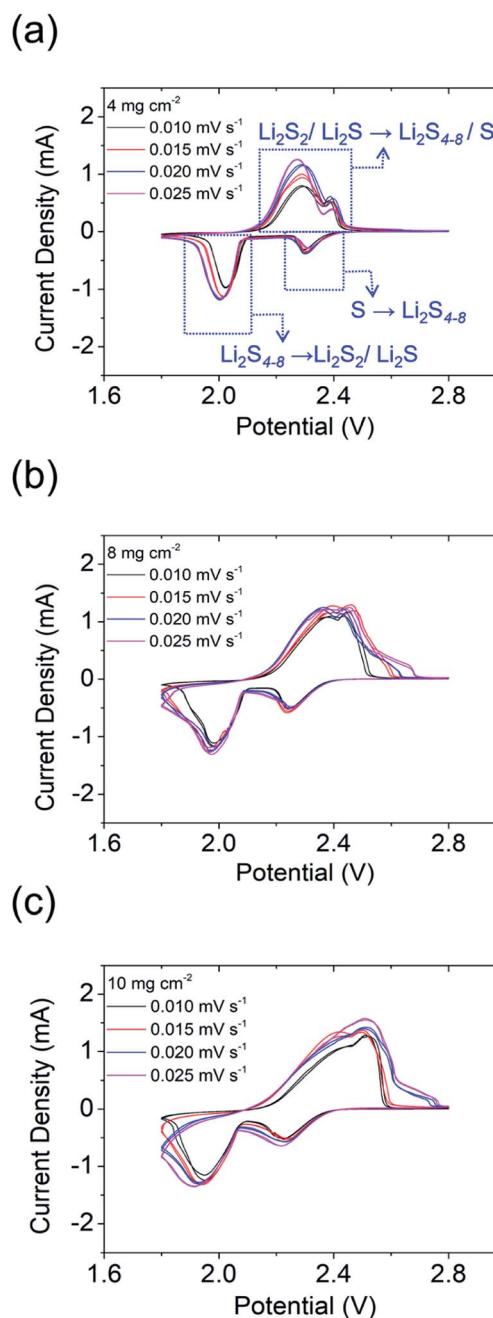
Fig. 4 Cyclic voltammograms of high-sulfur-loading cells: (a) 4 mg cm^{-2}; (b) 8 mg cm^{-2}; (c) 10 mg cm^{-2}.

aims to summarize the research trends in terms of cell-design parameters (i.e., sulfur loading and sulfur content) and the corresponding cell-electrochemical performances (i.e., the areal capacity and energy density), which together lighten the direction toward advanced lithium–sulfur batteries with a high-energy-density sulfur cathode and a high-performance safe GPE.

Specifically, as shown in Fig. 5a, the cells with the PMMA-based GPE enable the high-loading polysulfide cathodes to simultaneously attain high sulfur loading (10 mg cm^{-2}) and sulfur content (72 wt%), showing the improvement in the sulfur

13724 | J. Mater. Chem. A, 2022, **10**, 13719–13726

This journal is © The Royal Society of Chemistry 2022

(a)

(b)
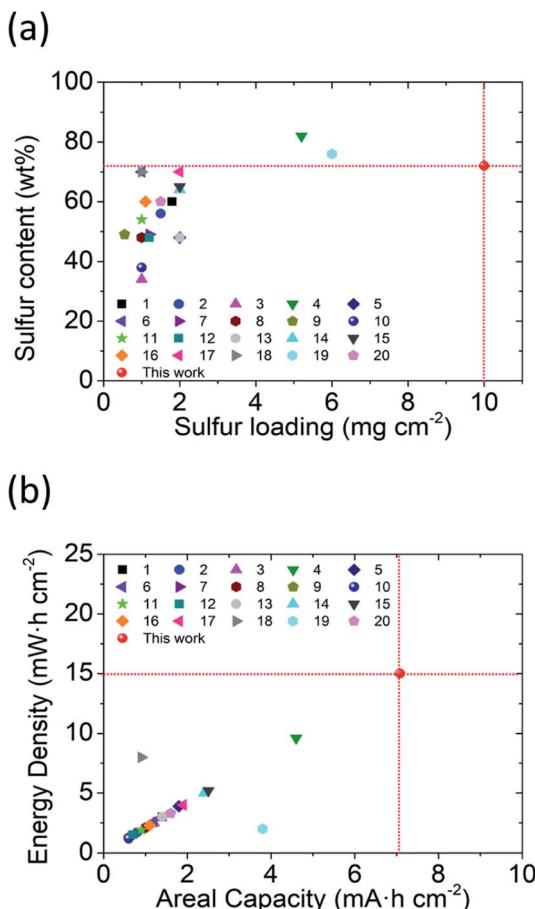
Fig. 5 Comparison of the cell-design parameters and cell-electrochemical performances of lithium−sulfur batteries with the PMMA-based GPE and other GPEs: (a) sulfur loading (mg cm^{-2}) and content (wt%) and (b) areal capacity (mA h cm^{-2}) and energy density (mW h cm^{-2}) based on the whole electrode.

cathode in the GPE system. Moreover, as shown in Fig. 5b, with such a high-loading polysulfide cathode, the PMMA-based GPE allows the enhanced electrochemical performance featuring a high areal capacity of 7.1 mA h cm^{-2} and excellent energy density of 15 mW h cm^{-2}, which promotes the development trend as compared to the previous studies. As a result, the comparison analysis shows a summary of various lithium–sulfur GPEs. The analytical results also demonstrate that our PMMA-based GPE attains the achievements in both cell design (*i.e.*, high sulfur loading and content) and cell performance (*i.e.*, outstanding areal capacity and energy density).

Conclusions

In this work, we mixed PMMA with LiTFSI on a polymeric separator matrix to form a PMMA-based GPE for developing lithium-sulfur cells with the direct use of a high-loading polysulfide cathode. First, we varied the concentration of the PMMA GPE and the LiTFSI salt. The high-loading polysulfide cathode with a PMMA-based GPE containing 90 wt% PMMA and 10 wt% LiTFSI exhibited the highest discharge capacities at a high

sulfur loading of 4 mg cm^{-2}. Moreover, the PMMA-based GPE exhibited the lowest impedance in EIS analysis. This proves that the addition of a suitable amount of LiTFSI can improve the ionic conductivity of GPEs and reduce the loss of active materials. Additionally, to achieve an energy storage system with a high energy density and areal capacity, we increased the sulfur loading to 8 and 10 mg cm^{-2}. The PMMA-based GPEs allowed the ultrahigh-loading polysulfide cathodes with 8 and 10 mg cm^{-2} sulfur to provide high initial discharge capacities of 797 and 708 mA h cm^{-2} at the *C*/10 rate, respectively, and excellent reversibility and rate performance after 100 cycles. Moreover, the cells with the high-sulfur-loading cathode benefitted from the PMMA-based GPE to achieve a high areal capacity and energy density of 7.1 mA h cm^{-2} and 15 mW h cm^{-2} at the *C*/10 rate, respectively. The results demonstrate that the PMMA-based GPE improved lithium-ion diffusion and prevented polysulfide diffusion. Therefore, the PMMA-based GPE improves the electrochemical stability and performance of high-sulfur-loading lithium–sulfur batteries.

Conflicts of interest

There are no conflicts to declare.

Acknowledgements

Notes and references

1 P. G. Bruce, S. A. Freunberger, L. J. Hardwick and J. M. Tarascon, *Nat. Mater.*, 2011, **11**, 19–29.

2 Y.-S. Su, Y. Fu, T. Cochell and A. Manthiram, *Nat. Commun.*, 2013, **4**, 2985.

3 S.-H. Chung and A. Manthiram, *Adv. Mater.*, 2019, **31**, 1901125.

4 A. Manthiram, Y. Fu and Y.-S. Su, *Acc. Chem. Res.*, 2013, **46**, 1125–1134.

5 G. Xu, B. Ding, J. Pan, P. Nie, L. Shen and X. Zhang, *J. Mater. Chem. A*, 2014, **2**, 12662–12676.

6 M. Zhao, B.-Q. Li, H.-J. Peng, H. Yuan, J.-Y. Wei and J.-Q. Huang, *Angew. Chem., Int. Ed.*, 2020, **59**, 12636–12652.

7 X. Ji, K. T. Lee and L. F. Nazar, *Nat. Mater.*, 2009, **8**, 500–506.

8 Y.-J. Quay and S.-H. Chung, *Nanomaterials*, 2021, **11**, 3342.

9 A. Belgibayeva and I. Taniguchi, *J. Power Sources*, 2021, **484**, 229308.

This journal is © The Royal Society of Chemistry 2022

J. Mater. Chem. A, 2022, **10**, 13719–13726 | **13725**

10 C.-S. Cheng and S.-H. Chung, *Chem. Eng. J.*, 2022, **429**, 132257.

11 Y. Yang, G. Yu, J. J. Cha, H. Wu, M. Vosgueritchian, Y. Yao, Z. Bao and Y. Cui, *ACS Nano*, 2011, **5**, 9187–9193.

12 S. Evers and L. F. Nazar, *Acc. Chem. Res.*, 2013, **46**, 1135–1143.

13 P. Zhu, J. Zhu, C. Yan, M. Dirican, J. Zang, H. Jia, Y. Li, Y. Kiyak, H. Tan and X. Zhang, *Adv. Mater.*, 2018, **5**, 1701598.

14 F.-J. Lai, L.-L. Chiu, C.-L. Lee, W.-Y. Lu, Y.-C. Lai, S. Ding, H.-Y. Chen and K.-H. Wu, *Polymer*, 2019, **182**, 121812.

15 J.-Q. Huang, Q. Zhang and F. Wei, *Energy Storage Mater.*, 2015, **1**, 127–145.

16 X. Judez, H. Zhang, C. Li, G. G. Eshetu, J. A. González-Marcos, M. Armand and L. M. Rodriguez-Martinez, *J. Electrochem. Soc.*, 2017, **165**, A6008–A6016.

17 D. Zhou, D. Shanmukaraj, A. Tkacheva, M. Armand and G. Wang, *Chem*, 2019, **5**, 2326–2352.

18 D. Lei, K. Shi, H. Ye, Z. Wan, Y. Wang, L. Shen, B. Li, Q.-H. Yang, F. Kang and Y.-B. He, *Adv. Funct. Mater.*, 2018, **28**, 1707570.

19 S. S. Zhang and D. T. Tran, *Electrochim. Acta*, 2013, **114**, 296–302.

20 L.-L. Chiu and S.-H. Chung, *Polymers*, 2021, **13**, 535.

21 Y.-C. Ho and S.-H. Chung, *Chem. Eng. J.*, 2021, **422**, 130363.

22 D. Yang, L. He, Y. Liu, W. Yan, S. Liang, Y. Zhu, L. Fu, Y. Chen and Y. Wu, *J. Mater. Chem. A*, 2019, **7**, 13679–13686.

23 P. M. Shanthi, P. J. Hanumantha, T. Albuquerque, B. Gattu and P. N. Kumta, *ACS Appl. Energy Mater.*, 2018, **1**, 483–494.

24 H. Du, S. Li, H. Qu, B. Lu, X. Wang, J. Chai, H. Zhang, J. Ma, Z. Zhang and G. Cui, *J. Membr. Sci.*, 2018, **550**, 399–406.

25 K. Park, J. H. Cho, J.-H. Jang, B.-C. Yu, A. T. De La Hoz, K. M. Miller, C. J. Ellison and J. B. Goodenough, *Energy Environ. Sci.*, 2015, **8**, 2389–2395.

26 H.-J. Peng, J.-Q. Huang, X.-B. Cheng and Q. Zhang, *Adv. Energy Mater.*, 2017, **7**, 1700260.

27 M. Rana, S. A. Ahad, M. Li, B. Luo, L. Wang, I. Gentle and R. Knibbe, *Energy Storage Mater.*, 2019, **18**, 289–310.

28 Y. Hu, W. Chen, T. Lei, Y. Jiao, J. Huang, A. Hu, C. Gong, C. Yan, X. Wang and J. Xiong, *Adv. Energy Mater.*, 2020, **10**, 200082.

29 Y.-J. Yang, R. Wang, J.-X. Xue, F.-Q. Liu, J. Yan, S.-X. Jia, T.-Q. Xiang, H. Huo, J.-J. Zhou and L. Li, *J. Mater. Chem. A*, 2021, **9**, 27390.

30 Q. Yu, D. Chen, J. Liang, Y. Chu, Y. Wu, W. Zhang, Y. Li, L. Li and R. Zeng, *RSC Adv.*, 2014, **4**, 59498–59502.

31 Y. Guo, Y. Ouyang, D. Li, Y. Wei, T. Zhai and H. Li, *Energy Storage Mater.*, 2019, **16**, 203–211.

32 M. Armand, S. Grugeon, H. Vezin, S. Laruelle, P. Ribiere, P. Poizot and J. M. Tarascon, *Nat. Mater.*, 2009, **8**, 120–125.

33 K. J. Thomas, M. Sheeba, V. P. N. Nampoori, C. P. G. Vallabhan and P. Radhakrishnan, *J. Opt. A: Pure Appl. Opt.*, 2008, **10**, 055303.

34 M. Miroshnikov, H. Wang, N. K. Thangavel, K. Mahankali, S. Satapathy, K. Kato, G. Babu, K. P. Divya, L. M. R. Arava, P. M. Ajayan and G. John, *J. Phys. Chem. C*, 2020, **124**, 17939–17948.